

Optically- and thermally-driven huge lattice orbital and spin angular momenta from spinning fullerenes

G. P. Zhang*

Department of Physics, Indiana State University, Terre Haute, Indiana 47809, USA

Y. H. Bai

Office of Information Technology, Indiana State University, Terre Haute, Indiana 47809, USA

Thomas F. George

Departments of Chemistry & Biochemistry and Physics & Astronomy, University of Missouri-St. Louis, St. Louis, MO 63121, USA

(Dated: September 24, 2021)

arXiv:2109.11055v1 [cond-mat.mtrl-sci] 22 Sep 2021

Abstract

Lattice vibration in solids may carry angular momentum. But unlike the intrinsic spin of electrons, the lattice vibration is rarely rotational. To induce angular momentum, one needs to find a material that can accommodate a twisted normal mode, two orthogonal modes or excitation of magnons. If excitation is too strong, one may exceed the Lindemann limit, so the material melts. Therefore these methods are not ideal. Here, we theoretically propose a new route to phonon angular momentum in a molecular crystal C_{60} . We find that a single laser pulse is able to inject a significant amount of angular momentum to C_{60} , and the momentum transfer is helicity-dependent. Changing from right-circularly polarized light to left-circularly polarized light switches the direction of phonon angular momentum. On the ultrafast time scale, the orbital angular momentum change closely resembles the displacive excitation of coherent phonons, with a cosine-function dependence on time, different from the spin counterpart. Atomic displacements, even under strong laser excitation, remain far below the Lindemann criterion. Under thermal excitation, spinning C_{60} even at room temperature generates a huge angular momentum close to several hundred \hbar . Our finding opens the door to a large group of fullerenes, from C_{60} , C_{70} to their endohedral derivatives, where angular momentum can be generated through light or temperature. This paves the way to the phononic control electronic spin and harvesting thermal energy through phonon angular momentum.

PACS numbers: 42.65.Ky, 78.66.Tr

Keywords:

Nuclear vibration is ubiquitous and important to biological, chemical, and physical processes, ranging from photosynthesis¹, photoisomerization² to spin manipulation³⁻⁵. Microscopically, each material has its own vibrational normal modes. However, due to the symmetry constraint⁶, normal modes rarely have a rotational eigenvector, so the phonon angular momentum (PAM) is feeble. The concept of phonon spin is not new^{7,8}, and reemerged⁹. McLellan¹⁰ investigated PAM in a rotationally invariant harmonic model. Interest in PAM is more recent^{9,11-14}. It was shown that one may use an electric field¹⁵ or temperature gradient¹⁶ to control PAM. By coupling PAM to the electronic spin degrees of freedom, one can use PAM to control spin devices¹⁷. However, the main obstacle is how to generate PAM in the first place. It was predicted that one could introduce chiral phonons in monolayer molybdenum disulfide¹⁸, but the real calculation¹⁹ showed that the effect is tiny in transition metal dichalcogenides. The same thing is true for Pt₃ and Pt₅²⁰, where the most of vibrational modes has nearly zero angular momentum, with the maximum close to $0.094(\hbar/2)$. Experimentally, it was demonstrated that one could construct a superimposed vibrational state which consists of two orthogonal vibrational modes to generate an artificial circular phonon mode²¹. One may also couple the phonon to magnons in a magnetic material²²⁻²⁵ to induce spin angular momentum of phonons, but one must first have magnons. In general, these methods are not easy.

Molecular crystals are different. The weak bonding between neighboring sites render atom motifs rotating freely. Buckminsterfullerene C₆₀²⁶ is a prime example. At room temperature, C₆₀ is spinning rapidly²⁷⁻²⁹ around its equilibrium lattice positions. Spinning is temperature-dependent. As temperature cools down below 261 K, the rotation slows down, where ¹³C NMR spectra of solid C₆₀ show a significant broadening at a chemical shift of 143 ppm^{27,30,31}. Its rotation can also be manipulated through substrates^{32,33}, the tip of scanning tunneling microscope³⁴ and encapsulation inside carbon nanotubes³⁵. C₆₀ rotation also affects its energy spectrum³⁶ and vibrational spectra³⁷. C₆₀ and C₇₀ are not the only fullerenes that spin. Endohedral fullerenes³⁸, with additional atoms encapsulated inside fullerenes, offer additional kinds of rotational dynamics³⁹, with applications to organic photovoltaic devices⁴⁰ and quantum computing⁴¹. Recently, possible light-induced superconductivity was reported in K₃C₆₀⁴². It is conceivable that light can inject angular momentum into K₃C₆₀. These readily available molecular crystals represent a new frontier for phonon angular momentum investigation.

In this Letter, instead of relying on artificial rotational motion of atoms to search for phonon angular momentum, we start with a material that rotates in the first place at room temperature. Specifically, we employ C_{60} as an example, and we show that a laser pulse can induce a significant orbital and spin angular momentum change. PAM depends on the laser helicity. Circularly polarized light injects more angular momentum to the system than linearly polarized light. Changing from right- to left-circularly polarized light switches angular momentum direction. The total angular momentum exactly follows the energy change, thus reaffirming that it is physical. The orbital and spin angular momenta depend on time differently. The orbital has a cosine dependence, very similar to dispersive excitation of coherent phonons⁴³. The lattice distortion of C_{60} is small even under strong laser excitation, with the atom displacement far below the Lindemann criterion⁴⁴. The global rotation of C_{60} generates several hundred of \hbar . Our finding here represents a different direction for phonon angular momentum research, and is expected to motivate experimental and theoretical investigations.

We define the total angular momentum of C_{60} as

$$\mathbf{J} = \sum_i \mathbf{j}_i(t) = \sum_i \mathbf{r}_i(t) \times \mathbf{p}_i(t), \quad (1)$$

where $\mathbf{p}_i(t)$ is its momentum of atom i at time t and $\mathbf{r}_i(t)$ is its position vector. The reason why we use \mathbf{J} instead of \mathbf{L} will become clear below. Although we do not quantize the atomic vibration formally here, we still use phonons below. To find the initial coordinates $\{\mathbf{r}_i(0)\}$ of carbon atoms in C_{60} , we use the spiral generation method proposed by Fowler and Manolopoulos⁴⁵ for the topological problem of fullerenes. Here, in brief, we first construct the adjacency matrix, and diagonalize it. The three lowest eigenvectors correspond to the x , y and z coordinates of the carbon atoms, and then we properly rescale them according to the radius of C_{60} .

To optimize the geometry, we employ the Su-Schrieffer-Heeger (SSH) model⁴⁶ often used in conjugated polymers, where only π electrons are treated quantum mechanically, and the nuclear motions are described by the classical potentials⁴⁷ since the mass of carbon atoms is more than three orders of magnitude larger than that of the electron. Recently, the SSH model finds an important application in topological insulators⁴⁸. The Hamiltonian reads^{49–51}

$$H_0 = - \sum_{\langle ij \rangle, \sigma} t_{ij} (c_{i, \sigma}^\dagger c_{j, \sigma} + h.c.) + \frac{K_1}{2} \sum_{\langle ij \rangle} (r_{ij} - d_0)^2 + \frac{K_2}{2} \sum_i \delta\theta_{i,p}^2 + \frac{K_3}{2} \sum_i (\delta\theta_{i,h,1}^2 + \delta\theta_{i,h,2}^2), \quad (2)$$

where $c_{i,\sigma}^\dagger$ is the electron creation operator at site i with spin $\sigma(=\uparrow\downarrow)$ ⁵² and the summation $\langle ij \rangle$ over $i(j)$ runs from 1 to 60 with $i \neq j$. The first term on the right-hand side represents the electron hopping between nearest-neighbor atoms at positions \mathbf{r}_i and \mathbf{r}_j , $t_{ij} = t_0 - \alpha(|\mathbf{r}_i - \mathbf{r}_j| - d_0)$, where $r_{ij} = |\mathbf{r}_i - \mathbf{r}_j|$, t_0 is the average hopping constant, and α is the electron-lattice coupling constant. The last three terms are the lattice stretching, pentagon-hexagon and hexagon-hexagon bending energies, respectively, (see further details in⁵³). You *et al.*⁵⁴ parametrized the Hamiltonian by fitting the energy gap, bond lengths and 174 normal mode frequencies to their respective experimental values. They found that $t_0 = 1.91$ eV, $\alpha = 5.0$ eV/Å, $K_1 = 42$ eV/Å², $K_2 = 8$ eV/rad², $K_3 = 7$ eV/rad² and $d_0 = 1.5532$ Å. These parameters are consistent with the literature values⁵⁵⁻⁶². With You's six parameters and with the electrons initially occupying 30 lowest energy levels, we optimize the structure. Figure 1(a) shows a two-dimensional structure of our optimized C₆₀, where the z axis is out of the page. The C₆₀ molecule has the highest I_h point symmetry. 60 carbon atoms form 90 bonds, 60 single bonds around 12 pentagons, and 30 single bonds shared by 20 hexagons (see Fig. 1(a)). Our double bond length is 1.403 Å, and the single bond length is 1.443 Å, both of which indeed match the experimental values of 1.40 ± 0.015 Å and 1.45 ± 0.015 Å^{63,64}. Figure 1(b) shows the energy spectrum with the degeneracy. The highest occupied molecular orbital (HOMO) is a H_u state, while the lowest unoccupied molecular orbital (LUMO) is a T_{1u} state. The first dipole-allowed transition is between HOMO and LUMO+1, which is highlighted by the double arrow. All these features are fully consistent with the prior study⁵⁴. The challenge is to fit 174 normal mode frequencies⁶⁵ with only six parameters. We find that the calculated frequencies within our theory slightly deviate from the experimental values⁶⁵ within 3%. For instance, our breathing mode $A_g(1)$ frequency is 481 cm⁻¹, while the experimental one is between 492²⁸ and 496⁶⁵ cm⁻¹. Our pentagonal pinch mode $A_g(2)$'s frequency is 1477 cm⁻¹, while the experimental one is 1470^{28,65} cm⁻¹. Here the error is 0.5%. Because our Hamiltonian does not include high-order terms⁶⁶, these small differences are expected and do not affect our main conclusion of the paper. For this reason, we do not adjust those parameters.

As seen above, there are varieties of ways to induce angular momentum change. We perturb the system with an ultrafast laser pulse, whose interaction with C₆₀ is described by

$$H_I = -e \sum_{i\sigma} \mathbf{E}(t) \cdot \mathbf{r}_i n_{i\sigma} , \quad (3)$$

where $\mathbf{E}(t)$ is the electric field of the laser and $n_{i\sigma}$ is the electron number operator at site i . We choose a Gaussian pulse for $\mathbf{E}(t)$: $\mathbf{E}(t) = A_0 \exp(-t^2/\tau^2)[\cos(\omega t)\hat{x} + \epsilon \sin(\omega t)\hat{y}]/\sqrt{1 + \epsilon^2}$, where A_0 , ω , τ , t , ϵ and τ are the field amplitude, laser frequency, pulse duration or width, time, helicity and pulse duration, respectively. \hat{x} and \hat{y} are the unit vectors along the x and y axes, respectively. We ensure that A_0 is large enough, so the quantum effect of light is small and the classical treatment of our laser field is adequate. We treat the electrons quantum mechanically through the time-dependent Liouville equation^{51,52},

$$i\hbar \frac{\partial \langle \rho_{ij}^\sigma \rangle}{\partial t} = \langle [H, \rho_{ij}^\sigma] \rangle, \quad (4)$$

where $H = H_0 + H_I$, and ρ_{ij}^σ is the density matrix. The lattice vibrations are described by the Newtonian equation. This classical treatment of nuclear motion is reasonable if the de Broglie wavelength is smaller than the system size, but if the de Broglie wavelength becomes comparable to the system size, then our approach is less accurate. We solve the coupled Liouville and Newtonian equations numerically.

We excite C_{60} with a 60-fs laser pulse with electric field amplitude of 0.01 V/Å. The photon energy is 2.76 eV, which is tuned to be resonant with the transition between HOMO and LUMO+1 (see Fig. 1b). Figure 2(a) displays the total energy (thin line), lattice kinetic energy (thick line) and lattice potential energy (thick dashed line) as a function of time. The curve around zero denotes the laser pulse. Upon laser excitation, energy enters the electronic system first. The peak in the total energy is mainly due to the electron energy. Through the electron-lattice interaction and laser excitation, the lattice starts to vibrate. Most of the lattice energy is in the potential energy, and the kinetic energy is very small. In the figure, we multiply the kinetic energy by 100. Carbon atoms move at a speed of $10^{-3} - 10^{-2}$ Å/fs, or 100-1000 m/s, very typical for nuclear vibrations. The oscillation is due to the energy exchange between the electron and lattice subsystems (for details, see⁵³). Since we want to check the energy conservation as well as vibrational oscillations, we do not dampen our system. We find that the oscillation has a period of 69.3 fs, which exactly matches the frequency of the breathing mode $A_g(1)$ ^{67,68}. Such a coherent phonon excitation has been observed experimentally⁶⁷ and in other systems as well⁴³. The reason why this $A_g(1)$ is excited strongly is due to our chosen laser parameters^{50,53}. Our interest is in the lattice angular momentum. Figure 2(b) shows the lattice angular momentum for three laser helicities (ϵ): right (σ^+), left (σ^-) and linear (π) pulses, with the polarization in the xy plane

(see Fig. 1(a)). There is a general trend as to how the angular momentum is transferred to the lattice. Upon laser excitation, the flow of angular momentum to the lattice occurs on the 100 fs time scale, which corresponds to the total energy absorbed. Although each atom still vibrates and exchanges its angular momentum with the rest of the atoms, the total angular momentum must remain constant and is conserved in the absence of an external field. This is rigorously reproduced in our calculation. The angular momentum shows a strong dependence on ϵ . For σ^- , the lattice angular momentum is along the $+z$ axis, while for σ^+ , it is along the $-z$ axis. The π pulse induces a much weaker angular momentum (see the long-dashed line). This is expected because the angular momentum of light is directly related to the helicity of light. When it interacts with C_{60} , the lattice angular momentum has the hallmark of incident light. Figures 2(c), (d) and (e) show the detailed change in J_x , J_y and J_z as a function of helicity ϵ . When $\epsilon = 0$, the laser polarization is linear along the x axis. One can see that only J_y differs from zero, because the atom moves mainly along the x axis. Going from $\epsilon = 0$ to 1, our pulse changes from a linearly polarized pulse to elliptically, and finally to a circularly polarized pulse. Both J_x and J_z increase significantly as the atom also moves along the y axis. J_z is negative as expected. When we change ϵ from 0 to -1, we have a left elliptically to circularly polarized pulse, so J_z flips its sign, fully consistent with our finding in Fig. 2(b).

What is unknown or less familiar is whether and how the lattice angular momentum \mathbf{J} can characterize a system. This is an important conceptual question because angular momentum is rarely used to characterize the dynamics of a system, except in atoms and some simple structures. Prior studies^{9,11-14} are all based on this assumption. We compare \mathbf{J} against the absorbed energy ΔE into C_{60} . When the laser photon energy is off resonance, the energy change follows the perturbative path and has a simple dependence on the laser field amplitude A_0 ⁶⁹, so the agreement between the angular momentum \mathbf{J} and ΔE could be coincidental. The harder question is what happens if the laser is on resonance. Figure 3(a) shows the energy absorbed as a function of laser field amplitude where the photon energy is tuned to the dipole-allowed transition between the HOMO and LUMO+1 states (Fig. 1(b)). It is clear that the dependence on A_0 is highly nonlinear. When A_0 is far below 0.005 V/Å, the change is linear, but as far as it closes to 0.005 V/Å, it peaks, after which it starts to decrease. Because resonant excitation activates multiple real electronic excitation, this opens other channels and ΔE decreases. Once A_0 exceeds 0.01 V/Å, ΔE increases again,

which is consistent with our prior study⁴⁹. Figure 3(b) is our angular momentum. One can see that its change with A_0 matches the absorbed energy change, down to some minor details. This proves that \mathbf{J} is physical, and it represents the acquired angular momentum from light.

It has been proposed that if one rewrites $\mathbf{r}(t)$ as a sum of the equilibrium position $\mathbf{r}_i(0)$ and the displacement $\mathbf{u}_i(t)$, $\mathbf{r}_i(t) = \mathbf{r}_i(0) + \mathbf{u}_i(t)$, the angular momentum for atom i can be separated into two terms:

$$\mathbf{j}_i(t) = \mathbf{r}_i(0) \times \mathbf{p}_i(t) + \mathbf{u}_i(t) \times \mathbf{p}_i(t) \equiv \mathbf{l}_i(t) + \mathbf{s}_i(t). \quad (5)$$

$\mathbf{l}_i(t)$ is called the orbital angular momentum of atom i , while $\mathbf{s}_i(t)$ is called the spin angular momentum^{3,9,10,12} because \mathbf{s}_i is independent of the initial position of an atom. By separating orbital from spin angular momentum, we can directly investigate the interplay between spin and orbital angular momenta on an ultrafast time scale.

Figure 3(c) compares the spin angular momentum with the orbital counterpart. We employ a 60-fs laser pulse with $\hbar\omega = 2.76$ eV and $A_0 = 0.01\text{V}/\text{\AA}$. We notice that the angular moment mainly enters the orbital part. From Eq. 5, we see that it is the momentum \mathbf{p}_i that is mainly responsible for this increase. S_z is very small and magnified by 10 in the figure. What is interesting is that the spin angular momentum does not follow the laser pulse, very different from the orbital angular momentum. The reason for this difference is straightforward. S_z depends on both $\mathbf{u}_i(t)$ and \mathbf{p}_i . Although the pulse peaks at 0 fs, the atom cannot follow instantaneously and needs time to respond. The behavior of L_z is like a cosine function, with its maximum at 0 fs, similar to displacive excitation of coherent phonons (DECP)⁴³. But S_z is like a sine function. The sum of S_z and L_z is J_z , which is constant after the laser field is gone because the system does not have a way to exchange angular momentum. This demonstrates that our definition of angular momentum through Eq. 5 is physically sound.

It has been a big challenge to induce phonon spin angular momentum in real materials^{19,21,22}. We can increase spin angular momentum by tuning the laser photon energy to vibrations directly¹⁷. We choose $\hbar\omega = 0.185$ eV, or 44.7 THz, to be resonant with nuclear vibrations. The laser pulse duration is also 60 fs and the field amplitude is increased to 0.15 V/ \AA . We caution that our current treatment of nuclear vibration may not be adequate to compute the infrared spectrum since we do not include the nuclear dipole moment and the

nuclear vibration is not treated quantum mechanically. Figure 3(d) shows that S_z reaches $0.5\hbar$. Under our laser field, the structure of C_{60} is well maintained, far below the Lindemann criterion⁴⁴ for melting. This criterion has been a major obstacle for a prior study¹⁹, where the atomic displacements for BaO and LiNbO₃ can be as large as 0.1 Å. Therefore, an experimental test is difficult.

The top figure of Fig. 4 shows atomic displacements projected on the xy plane for five atoms on the front pentagon. The scales for the x and y axes are increased by 100 for an easy view. One can see the displacement is well below the Lindemann criterion. This paves the way to experimental testing. What is even more interesting is that besides these internal rotations, under thermal excitation, the entire molecule spins rapidly, although along arbitrary axes at room temperature. The angular momentum is $L = I\Omega$, where I is the moment of inertia of C_{60} and Ω is the angular speed. Assuming C_{60} spins along the z axis through two pentagons (see Fig. 1), the moment of inertia is $I_z = m \sum_{i=1}^{60} (x_i^2 + y_i^2)$, where m is the mass of carbon atom and x_i and y_i are the coordinates of atom i . Note that the moment of inertia is almost identical along other axes because C_{60} is highly spherical. An early estimate puts Ω between 1.5/ps and 2.8/ps⁷⁰. According to the latest theoretical estimate²⁹, its average angular frequency is 0.34 rad/ps. Since our present study only contains one single C_{60} and has no intermolecular interaction between several fullerenes, we are unable to verify their average angular frequency. Instead, we use their number and find $|\mathbf{J}|$ for C_{60} to be $322\hbar$. This angular momentum is from the global rotation of C_{60} . Because our Hamiltonian in Eq. 2 only depends on the distance between neighboring atoms, the rapid global rotation of C_{60} does not enter our calculation directly and only implicitly through the laser field polarization. However, due to the high symmetry of C_{60} , different polarizations yield almost identical results. Therefore, the global rotation must be treated separately in our formalism. To see the thermal effect of the global rotation on the spin angular momentum, we set the initial velocities of the carbon atoms to $\sqrt{k_B T/m}$, where k_B is the Boltzmann constant and m is the carbon mass. We allow a random distribution of the initial velocity directions. We use four temperatures, $T = 0, 10, 150$ and 300 K.

The results are shown in the bottom figures of Fig. 4. Figure 4(a) is our result with 0 K, but with a small laser field amplitude of 0.01 V/\AA . The solid, dotted and long-dashed lines denote S_x , S_y , and S_z , respectively, and are the same for the rest of the figures. We see that only S_z has a sizable value. But as we increase temperature to 10 K, we find

that all the other components are increased to $0.5 \hbar$. The amplitude is comparable among all the three components. At 150 K, the spin increases to $5\hbar$. At room temperature of 300 K, Fig. 4(d) shows the spin angular momentum increases to $10\hbar$. We also check whether our initial configuration of velocity direction affects our results. Among all the configurations we investigate, we do not see any qualitative difference. They should be observable experimentally. Spinning C_{60} could be a natural phonon angular momentum generator. As a large group of other fullerenes are available and even its endohedral forms already exist, such as $N@C_{60}$ and $P@C_{60}$, our finding opens a new route to phonon angular momentum. The future study should focus on how to harvest such a huge momentum for technological applications.

In conclusion, we have proposed a route to generate phonon orbital and spin angular momenta from C_{60} , without resorting to more complicated synthetic methods^{18,19,21,22}. We show that a single laser pulse can transfer a significant amount of angular momentum to C_{60} . The phonon angular momentum that C_{60} receives shows a strong dependence on laser helicity. The circularly polarized light injects more momentum than the linearly polarized light. We demonstrate that the total angular momentum change follows the total energy change faithfully, thus establishing that even in the time domain PAM is a valid concept and can be used to characterize the system property. The orbital angular momentum is normally larger than the spin counterpart, and it also has a different dependence on time. Similar to DECP⁴³, the orbital has a cosine function dependence, while the spin has a sine function dependence. We find that the atomic displacement is spiral and its amplitude is far below the Lindemann criterion, which has been a big obstacle to a prior study¹⁹. The angular momentum of the entire C_{60} reaches $322 \hbar$ at room temperature. Since endohedral fullerenes such as $N@C_{60}$ and $P@C_{60}$ are readily available, our study points out a large group of materials suitable for phonon angular momentum generation. It is expected that our finding will motivate experimental and theoretical investigations in this field and beyond.

Acknowledgments

This work was solely supported by the U.S. Department of Energy under Contract No. DE-FG02-06ER46304. Part of the work was done on Indiana State University's high performance Quantum and Obsidian clusters. The research used resources of the National Energy

Research Scientific Computing Center, which is supported by the Office of Science of the U.S. Department of Energy under Contract No. DE-AC02-05CH11231.

* guo-ping.zhang@outlook.com. <https://orcid.org/0000-0002-1792-2701>

- ¹ T. Brixner, J. Stenger, H. M. Vaswani, M. Cho, R. E. Blankenship, and G. R. Fleming, Two-dimensional spectroscopy of electronic couplings in photosynthesis, *Nature* **434**, 625 (2005).
- ² F. Gai, K. C. Hasson, J. C. McDonald, and P. A. Anfirud, Chemical dynamics in proteins: the photoisomerization of retinal in bacteriorhodopsin, *Science* **279**, 1886 (1998).
- ³ D. A. Garanin and E. M. Chudnovsky, Angular momentum in spin-phonon processes, *Phys. Rev. B* **92**, 024421 (2015).
- ⁴ M. Fähnle, Th. Tsatsoulis, C. Illg, M. Haag, B. Y. Müller, and L. Zhang, Ultrafast demagnetization after femtosecond laser pulses: Transfer of angular momentum from the electronic system to magnetoelastic spin-phonon modes, *J. Supercond. Nov. Magn* **30**, 1381 (2017).
- ⁵ D. Zahn, F. Jakobs, Y. W. Windsor, H. Seiler, T. Vasileiadis, T. A. Butcher, Y. Qi, D. Engel, U. Atxitia, J. Vorberger and R. Ernstorfer, Lattice dynamics and ultrafast energy flow between electrons, spins, and phonons in a 3d ferromagnet, arXiv:2008.04611v1 (2020).
- ⁶ S. Coh, Classification of materials with phonon angular momentum and microscopic origin of angular momentum, arXiv:1911.05064v2 (2019)
- ⁷ S. V. Vonsovskii and M. S. Svirskii, Phonon spin, *Sov. Phys. Solid State* **3**, 1568 (1962).
- ⁸ A. D. Levine, A note concerning the spin of the phonon, *Nuovo Cimento* **26**, 190 (1962).
- ⁹ L. Zhang and Q. Niu, Angular momentum of phonons and the Einstein-de Haas effect, *Phys. Rev. Lett.* **112**, 085503 (2014).
- ¹⁰ A. G. McLellan, Angular momentum states for phonons and a rotationally invariant development of lattice dynamics, *J. Phys. C: Solid State Phys.* **21**, 1177 (1988).
- ¹¹ J. J. Nakane and H. Kohno, Angular momentum of phonons and its application to single-spin relaxation, *Phys. Rev. B* **97**, 174403 (2018).
- ¹² A. Rückriegel and R. A. Duine, Long-range phonon spin transport in ferromagnet-nonmagnetic insulator heterostructures, *Phys. Rev. Lett.* **124**, 117201 (2020).
- ¹³ S. Park and B.-J. Yang, Phonon angular momentum Hall effect, *Nano Lett.* **20**, 7694 (2020).
- ¹⁴ S. Streib, Difference between angular momentum and pseudoangular momentum, *Phys. Rev. B*

- 103**, L100409 (2021).
- ¹⁵ K. Moseni, R. Wilson, and S. Coh, Electric field control of phonon angular momentum in perovskite BaTiO₃, arXiv:2103.06316v1 (2021).
- ¹⁶ M. Hamada, E. Minamitani, M. Hirayama, and S. Murakami, Phonon angular momentum induced by the temperature gradient, *Phys. Rev. Lett.* **121**, 175301 (2018).
- ¹⁷ A. Stupakiewicz, C. S. Davies, K. Szerenos, D. Afanasiev, K. S. Rabinovich, A. V. Boris, A. V. Boris, A. V. Kimel, and A. Kirilyuk, Ultrafast phononic switching of magnetization, *Nat. Phys.* **17**, 489 (2021).
- ¹⁸ L. Zhang and Q. Niu, Chiral phonons at high-symmetry points in monolayer hexagonal lattices, *Phys. Rev. Lett.* **115**, 115502 (2015).
- ¹⁹ D. M. Juraschek and N. A. Spaldin, Orbital magnetic moments of phonons, *Phys. Rev. Materials* **3**, 064405 (2019).
- ²⁰ O. Bistoni, F. Mauri, and M. Calandra, Intrinsic vibrational angular momentum from nonadiabatic effects in noncollinear magnetic molecules, *Phys. Rev. Lett.* **126**, 225703 (2021).
- ²¹ T. F. Nova, A. Cartella, A. Cantaluppi, M. Först, D. Bossini, R. V. Mikhaylovskiy, A. V. Kimel, R. Merlin, and A. Cavalleri, An effective magnetic field from optically driven phonons, *Nat. Phys.* **13**, 132 (2017).
- ²² J. Holanda, D. S. Maior, A. Azevedo, and S. M. Rezende, Detecting the phonon spin in magnon–phonon conversion experiments, *Nat. Phys.* **14**, 500 (2018).
- ²³ S. Streib, H. Keshtgar, and G. E. W. Bauer, Damping of magnetization dynamics by phonon pumping, *Phys. Rev. Lett.* **121**, 027202 (2018).
- ²⁴ K. An *et al.*, Coherent long-range transfer of angular momentum between magnon Kittel modes by phonons, *Phys. Rev. B* **101**, 060407(R) (2020).
- ²⁵ A. Rückriegel, S. Streib, G. E. W. Bauer, and R. A. Duine, Angular momentum conservation and phonon spin in magnetic insulators, *Phys. Rev. B* **101** 104402 (2020).
- ²⁶ H. W. Kroto, J. R. Heath, S. C. O’Brien, R. F. Curl, and R. E. Smalley, C₆₀: Buckminsterfullerene, *Nature* **318**, 162 (1985).
- ²⁷ R. D. Johnson, C. S. Yannoni, H. C. Dorn, J. R. Salem, and D. S. Bethune, C₆₀ rotation in the solid state: Dynamics of a faceted spherical top, *Science* **255**, 1235 (1992).
- ²⁸ M. S. Dresselhaus, G. Dresselhaus, and P. C. Eklund, *Science of Fullerenes and Carbon Nanotubes*, Academic Press, San Diego, California (1996).

- ²⁹ A. M. Bubenchikov, M. A. Bubenchikov, D. V. Mamontov, and A. V. Lun-Fu, MD-simulation of fullerene rotations in molecular crystal fullerite, *Crystals* **9**, 496 (2019).
- ³⁰ R. Tycko, R. C. Haddon, G. Dabbagh, S. H. Glarum, D. C. Douglass, and A. M. Mujsce, Solid-state magnetic resonance spectroscopy of fullerenes, *J. Phys. Chem.* **95**, 518 (1991).
- ³¹ R. Tycko, G. Dabbagh, R. M. Fleming, R. C. Haddon, A. V. Makhija, and S. M. Zahurak, Molecular dynamics and the phase transition in solid C₆₀, *Phys. Rev. Lett.* **67**, 1886 (1991).
- ³² L.-L. Wang and H.-P. Cheng, Rotation, translation, charge transfer, and electronic structure of C₆₀ on Cu(111) surface, *Phys. Rev. B* **69**, 045404 (2004).
- ³³ S. I. Bozhko, S. A. Krasnikov, O. Lübben, B. E. Murphy, K. Radican, V. N. Semenov, H. C. Wu, B. Bulfin, and I. Shvets, Rotational transitions in a C₆₀ monolayer on the WO₂/W(110) surface, *Phys. Rev. B* **84**, 195412 (2011).
- ³⁴ N. Neel, L. Limot, J. Kröger, and R. Berndt, Rotation of C₆₀ in a single-molecule contact, *Phys. Rev. B* **77**, 125431 (2008).
- ³⁵ Y. Zou, B. Liu, L. Wang, D. Liu, S. Yu, P. Wang, T. Wang, M. Yao, Q. Li, B. Zou, T. Cui, G. Zou, T. Wagberg, B. Sundqvist, and H.-K. Mao, Rotational dynamics of confined C₆₀ from near-infrared Raman studies under high pressure, *PNAS* **106**, 22135 (2009).
- ³⁶ J. R. F. Lima, J. Brandao, M. M. Cunha, and F. Moraes, Effects of rotation in the energy spectrum of C₆₀, *Eur. Phys. J. D* **68**, 94 (2014).
- ³⁷ R. Saito, G. Dresselhaus, and M. S. Dresselhaus, Hindered rotation of solid ¹²C₆₀ and ¹³C₆₀, *Phys. Rev. B* **50**, 5680 (1994).
- ³⁸ D. S. Bethune, R. D. Johnson, J. R. Salem, M. S. de Vries, and C. S. Yannoni, Atoms in carbon cages: the structure and properties of endohedral fullerenes, *Nature* **366**, 123 (1993).
- ³⁹ J. Hernandez-Rojas, J. Breton, and J. M. G. Llorente, Rotational dynamics of endohedral C₆₀ fullerene complexes, *J. Phys. Chem. Solids* **58**, 1689 (1997).
- ⁴⁰ R. B. Ross, C. M. Cardona, D. M. Guldi, S. G. Sankaranarayanan, M. O. Reese, N. Kopidakis, J. Peet, B. Walker, G. C. Bazan, E. Van Keuren, B. C. Holloway, and M. Drees, Endohedral fullerenes for organic photovoltaic devices, *Nat. Mater.* **8**, 208 (2009).
- ⁴¹ J. Twamley, Quantum-cellular-automata quantum computing with endohedral fullerenes, *Phys. Rev. A* **67**, 052318 (2003).
- ⁴² M. Mitrano, A. Cantaluppi, D. Nicoletti, S. Kaiser, A. Perucchi, S. Lupi, P. Di Pietro, D. Pontiroli, M. Riccò, S. R. Clark, D. Jaksch, and A. Cavalleri, Possible light-induced supercon-

- ductivity in K_3C_{60} at high temperature, *Nature* **530**, 461 (2016).
- ⁴³ H. J. Zeiger, J. Vidal, T. K. Cheng, E. P. Ippen, G. Dresselhaus, and M. S. Dresselhaus, Theory for displacive excitation of coherent phonons, *Phys. Rev. B* **45**, 768 (1992).
- ⁴⁴ F. A. Lindemann, Über die Berechnung molekularer Eigenfrequenzen, *Phys. Z.* **11**, 609 (1910).
- ⁴⁵ P. W. Fowler and D. E. Manolopoulos, *An Atlas of Fullerenes*, Clarendon Press, Oxford (1995).
- ⁴⁶ W. P. Su, J. R. Schrieffer, and A. J. Heeger, Solitons in polyacetylene, *Phys. Rev. Lett.* **42**, 1698 (1979).
- ⁴⁷ A. J. Heeger, S. Kivelson, J. R. Schrieffer, and W. P. Su, Solitons in conducting polymers, *Rev. Mod. Phys.* **60**, 781 (1988).
- ⁴⁸ J. K. Asboth, L. Oroszlany and A. Palyi, A Short course on topological insulators: Band structure and edge states in one and two dimensions, *Lecture Notes in Physics*, Vol. **919**. Springer (2016).
- ⁴⁹ G. P. Zhang, X. Sun, and T. F. George, Laser-induced ultrafast dynamics in C_{60} , *Phys. Rev. B* **68**, 165410 (2003).
- ⁵⁰ G. P. Zhang and T. F. George, Controlling vibrational excitations in C_{60} by laser pulse durations, *Phys. Rev. Lett.* **93**, 147401 (2004).
- ⁵¹ G. P. Zhang, Optical high harmonic generations in C_{60} , *Phys. Rev. Lett.* **95**, 047401 (2005).
- ⁵² G. P. Zhang, Hartree-Fock dynamical electron-correlation effects in C_{60} after laser excitation, *Phys. Rev. Lett.* **91**, 176801 (2003).
- ⁵³ See Supplementary Material.
- ⁵⁴ W. M. You, C. L. Wang, F. C. Zhang, and Z. B. Su, Application of a Su-Schrieffer-Heeger-like model to the intramolecular electron-phonon coupling in C_{60} clusters, *Phys. Rev. B* **47**, 4765 (1993).
- ⁵⁵ G. B. Adams, J. B. Page, O. F. Sankey, K. Sinha, J. Menendez, and D. R. Huffman, First-principles quantum molecular-dynamics study of the vibrations of icosahedral C_{60} , *Phys. Rev. B* **44**, 4052(R) (1991).
- ⁵⁶ M. Menon and K. R. Subbaswamy, Universal Parameter Tight-Binding Molecular Dynamics: Application to C_{60} , *Phys. Rev. Lett.* **67**, 3487 (1991).
- ⁵⁷ J. L. Feldman, J. Q. Broughton, L. L. Boyer, D. E. Reich, and M. D. Kluge, Intramolecular-force-constant model for C_{60} , *Phys. Rev. B* **46**, 12731 (1992).
- ⁵⁸ J. C. R. Faulhaber, D. Y. K. Ko, and P. R. Briddon, Vibronic coupling in C_{60} and C_{60}^{-3} , *Phys.*

- Rev. B **48**, 661 (1992).
- ⁵⁹ B. Friedman, Infrared absorption of polarons in C_{60} , Phys. Rev. B **48**, 17551 (1993).
- ⁶⁰ K. Harigaya and S. Abe, Optical-absorption spectra in fullerenes C_{60} and C_{70} : Effects of Coulomb interactions, lattice fluctuations, and anisotropy, Phys. Rev. B **49**, 16746 (1994).
- ⁶¹ W.-Z. Wang, C.-L. Wang, Z.-B. Su, and L. Yu, Lattice relaxation study on self-trapped exciton and biexciton in neutral and charged fullerenes, Phys. Rev. Lett. **72**, 3550 (1994).
- ⁶² J. Liu, S. Iwata, and B. Gu, Structural properties of the endohedral complex $Na^+@C_{60}$, J. Phys.: Condens. Matter **6**, L253 (1994).
- ⁶³ K. Hedberg, L. Hedberg, D. S. Bethune, C. A. Brown, H. C. Dorn, R. D. Johnson, and M. de Vries, Bond lengths in free molecules of Buckminsterfullerene, C_{60} , from gas-phase electron diffraction, Science **254**, 410 (1991).
- ⁶⁴ C. S. Yannoni, P. P. Bernier, D. S. Bethune, G. Meijer and J. R. Salem. NMR determination of the bond lengths in C_{60} , J. Am. Chem. Soc. **113**, 3190 (1991).
- ⁶⁵ J. Menendez and J. B. Page, Vibrational spectroscopy of C_{60} , in *Light Scattering in Solids VIII Fullerenes, Semiconductor Surfaces, Coherent Phonons*, edited by M. Cardona and G. Güntherodt, Springer (2000).
- ⁶⁶ Z. C. Wu, D. A. Jelski, and T. F. George, Vibrational motions of Buckminsterfullerene, Chem. Phys. Lett. **137**, 291 (1987).
- ⁶⁷ S. L. Dexheimer, D. M. Mittleman, R. W. Schoenlein, W. Vareka, X.-D. Xiang, A. Zettl, and C. V. Shank, Ultrafast Dynamics of Photoexcited C_{60} , in *Ultrafast Pulse Generation and Spectroscopy*, edited by T. R. Gosnell, A. J. Taylor, K. A. Nelson, and M. C. Downer, SPIE Proc. **1861**, 328 (1993).
- ⁶⁸ G. P. Zhang and T. F. George, Normal-mode selectivity in ultrafast Raman excitations in C_{60} , Phys. Rev. B **73**, 035422 (2006).
- ⁶⁹ Y. R. Shen, *The Principles of Nonlinear Optics*, John Wiley & Sons, Inc., Hoboken, New Jersey (2003).
- ⁷⁰ Q.-M. Zhang, J.-Y. Yi, and J. Bernholc, Structure and dynamics of solid C_{60} , Phys. Rev. Lett. **66**, 2633 (1991).

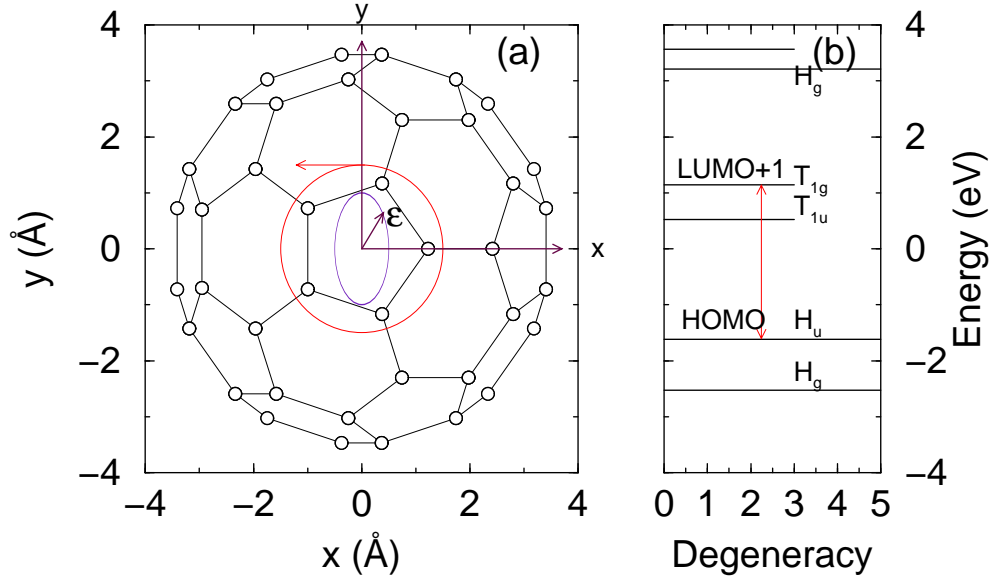


FIG. 1: (a) C₆₀ structure. The empty circles denote sixty carbon atoms. The laser polarization (the vector) is in the xy plane (the front pentagon) and controlled by the helicity ϵ . (b) Energy level scheme for C₆₀. The double-arrow denotes the transition between the second lowest unoccupied molecular orbital (LUMO+1) and highest occupied molecular orbital (HOMO).

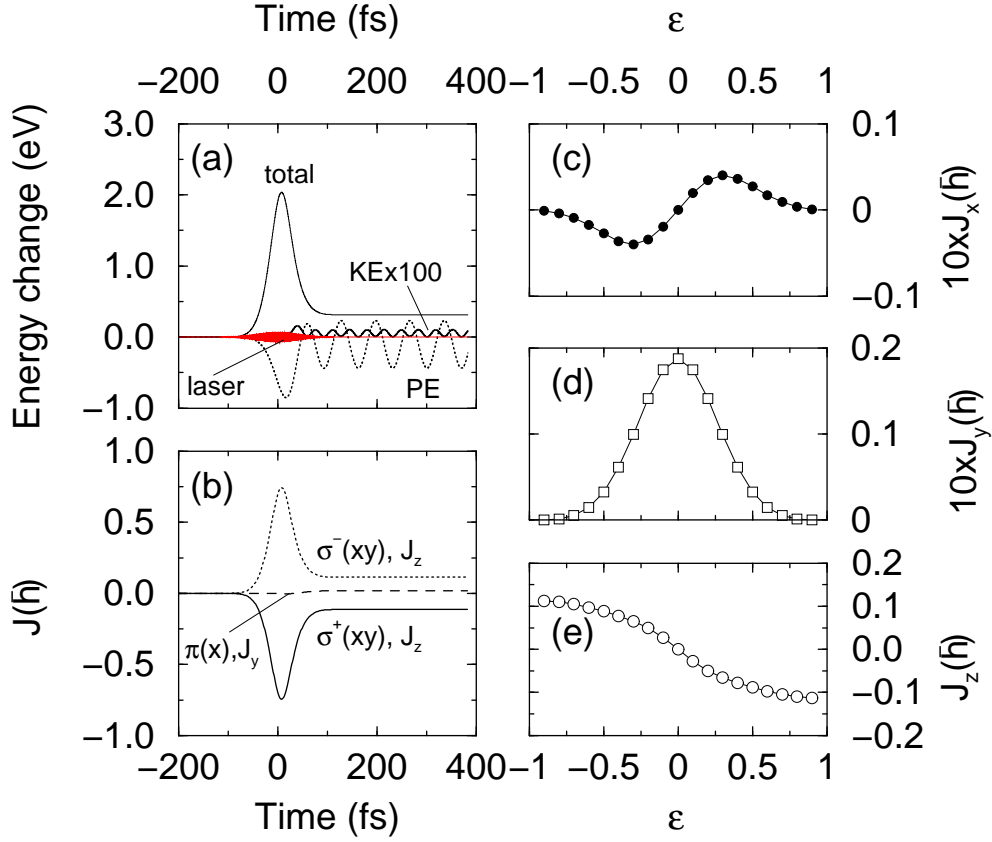


FIG. 2: (a) Total energy change as a function of time under a 60-fs σ^+ pulse. Here $\epsilon = 1$. The laser field amplitude is 0.01 V/\AA , and the photon energy is $\hbar\omega = 2.76 \text{ eV}$. Thin solid, thick solid, and dashed lines denote the system total energy, lattice kinetic and potential energy, respectively. The lattice kinetic energy is multiplied by 100 to have an easy view. To demonstrate the energy conservation, the system is not damped. The red thin line around 0 is the laser electric field. The oscillation period in the lattice potential is 69.3 fs, which exactly matches the frequency of the Raman-active $A_g(1)$ mode. (b) Total angular momentum \mathbf{J} under σ^+ (solid line), σ^- (dotted line) and π pulses (dashed line). Only the strongest component of \mathbf{J} is shown. Linearly polarized light transfers a small angular momentum. The left- and right-circularly polarized light transfer opposite angular momenta. All the pulses have the same laser parameters as (a). (c), (d) and (e) show the final x , y and z components of \mathbf{J} as a function of ellipticity ϵ .

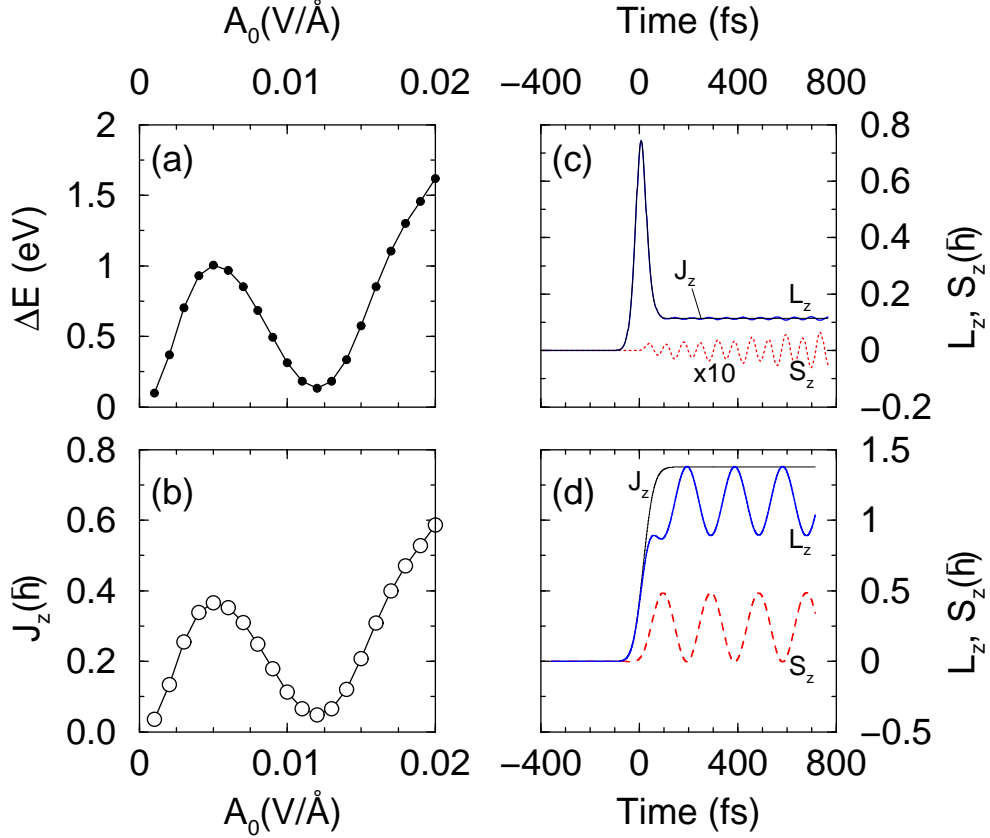


FIG. 3: (a) Absorbed energy ΔE as a function of laser field amplitude A_0 . The photon energy and pulse duration are the same as Fig. 2. (b) Total angular momentum as a function of laser field amplitude A_0 , which matches the total energy change. This demonstrates that \mathbf{J} is physical. (c) The orbital L_z and spin S_z angular momenta as a function of time. S_z is very small when $\hbar\omega = 2.76$ eV. In the figure, it is multiplied by 10. (d) The orbital L_z and spin S_z angular momenta as a function of time with $\hbar\omega = 0.185$ eV. S_z reaches a comparable magnitude as L_z . The dependence of S_z on time follows a sine function, while that of L_z follows a cosine function, very similar to DECP⁴³.

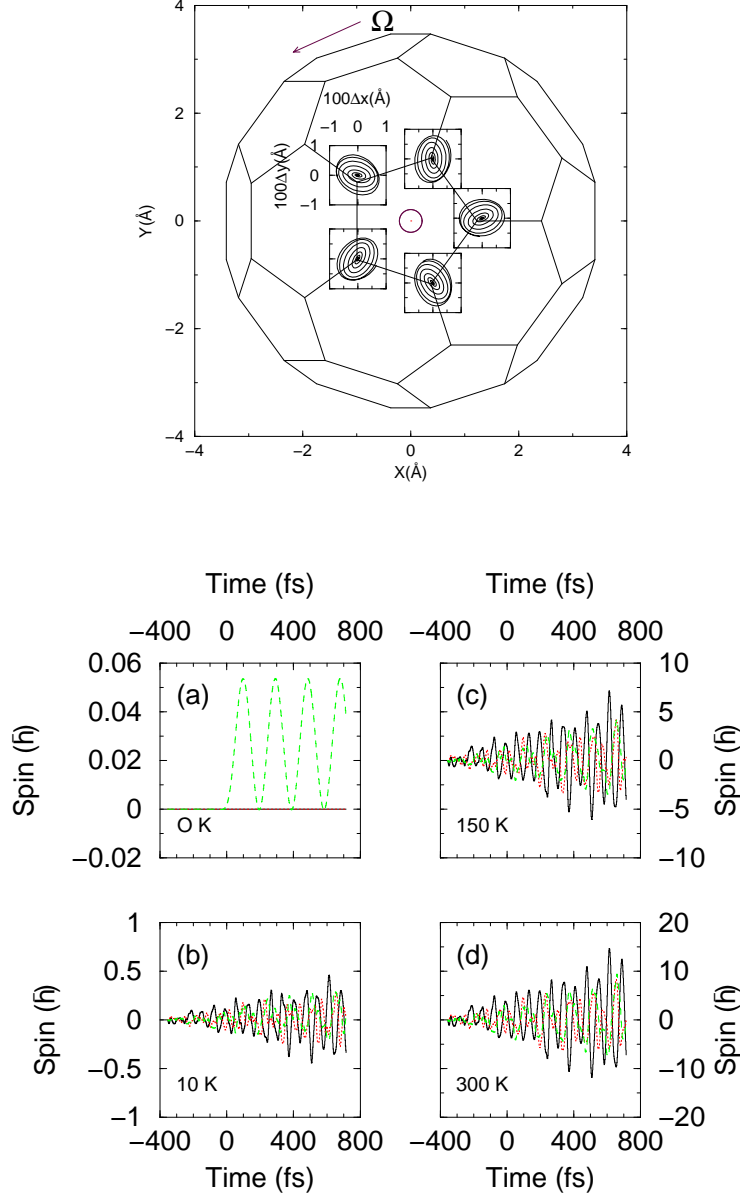


FIG. 4: (Top) Traces of displacements of five carbon atoms on the front pentagon in the earlier stage of laser excitation. The change is only 0.01 \AA , which is well below the Lindemann criterion⁴⁴. The arrow on the top left denotes the rotation of entire C₆₀. (Bottom) Phonon spin angular momentum at (a) 0 K, (b) 10 K, (c) 150 K and (d) 300 K, where the solid, dotted and long-dashed lines denote S_x , S_y and S_z , respectively. Its magnitude becomes larger as temperature increases.